Special Issue on APAMS 2026

ARTICLE

Highly hydrophobic behavior of SLA 3D-printed micropillar arrays with carnauba wax coating

Marco P. Rodriguez

Department of Science and Technology - Industrial Technology Development Institute, Bicutan, Taguig City, 1631 Philippines

ABSTRACT

This study presents the design and fabrication of highly hydrophobic micropillar arrays by stereolithography (SLA) 3D printing, with systematic variation of geometrical parameters to reduce surface wetting. Hydrophobicity depends on both surface roughness and surface chemistry. Microstructural features were therefore designed and produced by controlled 3D printing. The printer's limits on feature size and pillar spacing were first established at 200 µm. Three pillar shapes were evaluated: cylindrical, conical, and inverted conical. Conical pillars were printed with the highest fidelity, whereas cylindrical and inverted conical pillars were affected by light bleeding and unintended curing, which compromised their structure. The effects of pillar height and surface modification were then investigated. Samples were treated with alkali and coated with carnauba wax, a natural material with low surface energy. Wetting was quantified by static water contact angle measured with an optical tensiometer. Micro-scale roughness for 1000 µm pillar height combined with single wax coating raised the contact angle to a mean of 140.72° ± 12.84°, compared with 67.17° ± 3.91° for an uncoated flat surface. Three-dimensional microscopy gave an areal height parameter (Sa) of 173.03 µm and a root-mean-square height (Sq) of 210.29 µm for the best-performing sample, values dominated by the pillar height. Scanning electron microscopy showed differences in surface texture, pillar shape, and wax coverage, and Fourier-transform infrared spectroscopy identified the functional groups of the resin and the wax and the small changes after alkali treatment. Overall, SLA microstructuring combined with a carnauba wax coating is an effective way to make hydrophobic surfaces, although durability and dynamic wetting were not evaluated.

*Corresponding author
Email Address: **marco4138@gmail.com**
Date received: 15 June 2026
Dates revised: 30 July 2026; 07 September 2026
Date accepted: 23 September 2026
DOI: https://doi.org/10.54645/202619SupTRJ-14

INTRODUCTION

Surface wettability governs solid–liquid interactions and affects many applications, including self-cleaning coatings, anti-fouling and anti-corrosion systems, microfluidics, condensation control, and heat transfer. The wetting of a surface is commonly quantified by the static water contact angle (CA), which results from the balance of interfacial energies at the solid–liquid–vapor contact line. On ideal, smooth, and chemically homogeneous surfaces, the equilibrium contact angle is given by Young's equation (Young, 1805). Real surfaces deviate from this ideal because of roughness and chemical heterogeneity, which produce wetting regimes that Young's equation alone cannot describe. In the Wenzel state, the liquid fills the surface asperities, which increases the solid–liquid contact area and amplifies the intrinsic wetting behavior (Wenzel, 1936). In the Cassie–Baxter state, the liquid rests on a composite interface of solid and trapped air, which reduces the solid fraction in contact with the liquid and increases the apparent contact angle (Cassie and Baxter, 1944). These models describe two limiting cases, but the transition between them is not purely geometric: it depends on metastable energy barriers, local curvature, and perturbations such as droplet impact or pressure fluctuations. Keeping the Cassie–Baxter state stable is therefore a central challenge in designing hydrophobic surfaces. Consequently, maintaining a stable Cassie–Baxter state remains a central challenge in the design of hydrophobic surfaces. Surface structuring can be used to control wetting. Micropillar arrays are a good model system for studying how geometry affects wetting. Varying the pillar height, diameter, spacing, and aspect ratio changes the solid fraction and droplet mobility. Wetting transitions are highly sensitive to dimensions: small variations in the microstructure can trigger an irreversible collapse from the Cassie–Baxter to the Wenzel state under dynamic conditions, which shows that hydrophobicity based on air entrapment is fragile (Wang et al., 2022).

Additive manufacturing, particularly stereolithography (SLA) vat photopolymerization, has emerged as a way to fabricate such microstructures. SLA builds parts layer by layer by UV-induced

KEYWORDS

Hydrophobic surfaces, Stereolithography, Micropillar arrays, Carnauba wax, Additive manufacturing

photopolymerization, which allows direct fabrication of three-dimensional microstructures with high design flexibility. Compared with lithography and etching, SLA offers rapid prototyping and complex geometries that are otherwise difficult to make. Vat photopolymerization is increasingly used for functional surfaces, including microstructured interfaces for fluid control and wetting (Pagac et al., 2021)

However, the surface energy of methacrylate-based photopolymers limits SLA-printed surfaces: even when microstructured, they are only weakly hydrophobic or hydrophilic. Topography alone therefore cannot stabilize a hydrophobic state. In practice, incomplete air trapping and low energy barriers lead to partial wetting and a transition to the Wenzel state under realistic conditions (Pathreeker et al., 2021). A chemical surface modification is therefore needed to lower the surface energy of the base material.

Low-surface-energy coatings can overcome this limitation. Among them, bio-based waxes are attracting interest as alternatives to fluorinated compounds because they are non-toxic, low in cost, and compatible with simple coating processes. Carnauba wax, which consists mainly of long-chain aliphatic esters and hydrocarbons, has a low surface energy and can greatly reduce liquid adhesion on structured substrates (Gupta et al., 2021). On micro- or nanostructured surfaces, such coatings help to retain air within the features and stabilize the Cassie–Baxter state, which raises the apparent contact angle (Saji, 2020).

Earlier studies have shown that stereolithography can produce microstructured surfaces with enhanced water repellency. Bonilla-Cruz et al. (2021) fabricated superhydrophobic (>150°) µ-pillars with fluorinated alkylsilane coating and showed the importance of the staircase effect and pillar geometry. Wu et al. (2022) studied fluorosilane-treated microcylindrical arrays, achieving a maximum water contact angle of 143.6° at a cylinder diameter of 30 µm and an inter-cylinder spacing of 90 µm. These studies focused on the relationship between the printed microstructure and wetting. However, the combined effect of printed micropillar geometry and a bio-based wax coating on wetting has not been studied.

This study investigates micropillar arrays combined with a carnauba wax coating to increase hydrophobicity. The novelty of this work is the combined evaluation of SLA-printed micropillars, surface treatment, and carnauba wax deposition, and their effects on wetting and three-dimensional topography. The study compares untreated, alkali-treated, single-wax-coated, and double-wax-coated surfaces. Morphology and three-dimensional topography are characterized by scanning electron microscopy (SEM) and 3D digital microscopy, and chemical changes after alkali treatment and wax coating by Fourier-transform infrared (FTIR) spectroscopy.

MATERIALS AND METHODS

Materials

Microstructured samples were printed by stereolithography from a methacrylate-based photosensitive resin (BioMed Clear, Formlabs Inc.). Analytical-grade sodium hydroxide (NaOH; Sigma-Aldrich) was used for the alkali surface treatment. Type 1 carnauba wax (from *Copernicia cerifera*; Dalkem Corporation) was used as the low-surface-energy coating. Based on manufacturer, carnauba wax consists mainly of long-chain aliphatic esters, fatty acids, and hydrocarbons and melts at 81–86 °C, which makes it suitable for application as a film on microstructured surfaces.

Design and Fabrication of Micropillar Arrays

Micropillar arrays were designed in Onshape CAD software and exported as STL files to the PreForm slicing software. The arrays were printed on a Formlabs Form 2 SLA printer with a 405 nm laser wavelength, 250 mW power, 140 µm spot size, and a 25 µm layer thickness setting.

Three pillar geometries (cylindrical, conical, and inverted conical) were initially evaluated. Conical pillars were selected as the main geometry because of their structural stability and print fidelity: they are less likely to collapse at high aspect ratios and are more robust under capillary and drying forces (see Micropillar Geometry in the Results).

Table 1: Geometrical design parameters (levels) of the micropillar arrays.

Factor	Level 1	Level 2	Level 3	Level 4	Level 5
Pillar Height (µm)	200	400	600	800	1000
Bottom Diameter (µm)	200	300	-	-	-
Top Diameter (µm)	200	300	-	-	-
Bottom Spacing Edge-to-Edge (µm)	100	200	300	400	-
Orientation	0°	30°	-	-	-

Table 1 lists the parameters that were varied: pillar height (200–1000 µm), bottom diameter (200 and 300 µm), top diameter (200 and 300 µm), spacing (100–400 µm), and build orientation (0° and 30°). The listed levels define three geometries: a cone with a 300 µm bottom diameter and a 200 µm top diameter, a cylinder with equal diameters, and an inverted cone with a 200 µm bottom diameter and a 300 µm top diameter. The final printed configuration (Figure 1) consisted of conical micropillars with a bottom diameter of 300 µm, a top diameter of 200 µm, and heights from 200 to 1000 µm, printed at a 30° build orientation about the y-axis. The bottom spacing (clearance) was 200 µm along the x-axis and 300 µm along the y-axis, with respective pitch distances of 500 µm and 600 µm.

After printing, the samples were post-processed to preserve structural fidelity. Post-processing consisted of ultrasonic washing in 99% isopropyl alcohol (IPA) for 10 min to remove uncured resin, followed by air drying for 60 min. Supports were removed after washing. The samples were then post-cured at 60 °C for 60 min in a Form Cure UV post-curing system (405 nm) to complete crosslinking and stabilize their mechanical properties.

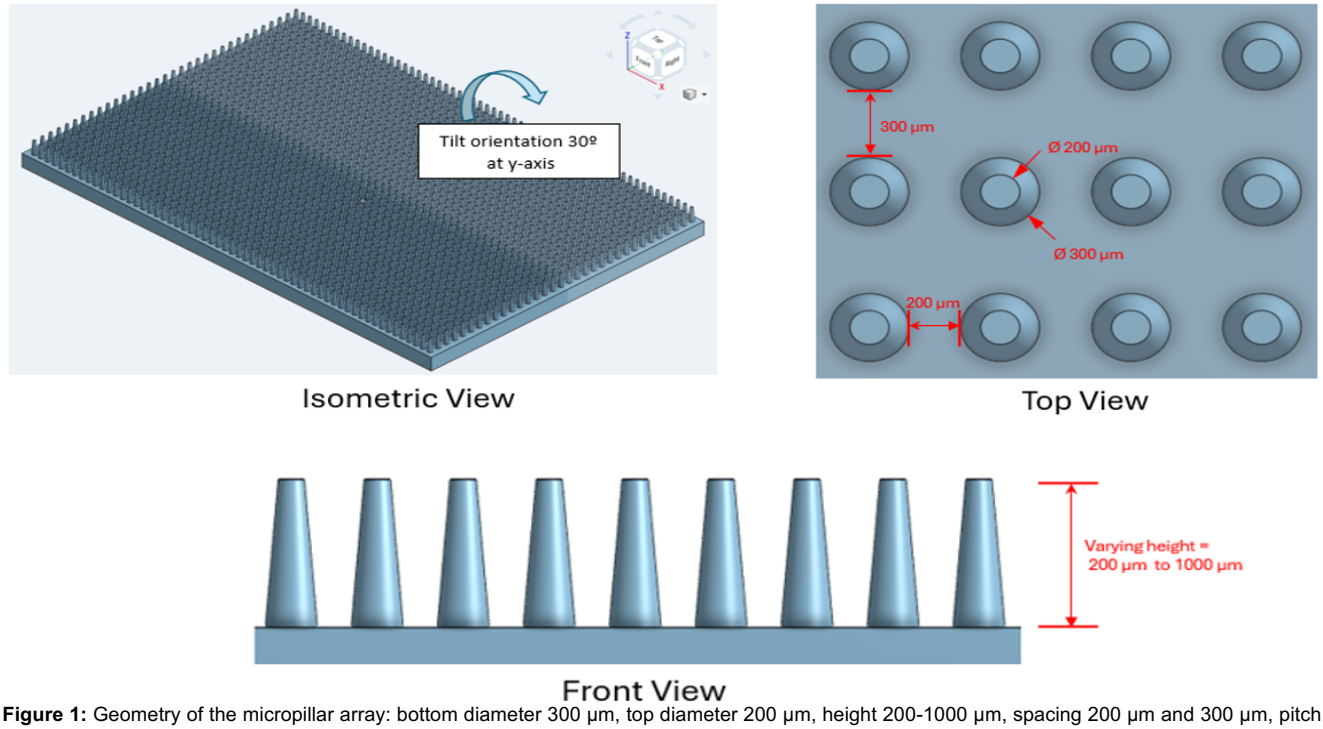


Figure 1: Geometry of the micropillar array: bottom diameter 300 µm, top diameter 200 µm, height 200-1000 µm, spacing 200 µm and 300 µm, pitch 500 µm and 600 µm, build orientation 30°.

Alkali Surface Treatment

The alkali treatment was performed in a 5 wt% aqueous NaOH solution for 1 h at 25 °C. This step was intended to modify the surface morphology by partial hydrolysis and etching of the methacrylate-based polymer network. Hydroxide ions are known to attack the ester groups of methacrylate polymers and to degrade their surface (Sandner and Bischof, 1983), a mechanism assumed to apply to the present crosslinked photopolymer. After treatment, the samples were rinsed with distilled water for 10 min and air-dried at room temperature for 60 min.

Carnauba Wax Coating

The carnauba wax coating was applied by a thermally induced infiltration–solidification process (Figure 2). The samples were embedded in 3 grams of wax powder in an aluminum pan so that the molten wax would be in full contact with the upright micropillar network.

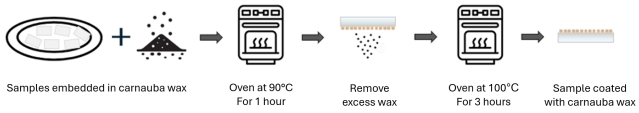


Figure 2: Schematic of the carnauba wax coating process, showing the thermal infiltration and solidification stages

A two-step thermal procedure was used: (i) heating at 90 °C for 1 h to melt the wax and promote capillary infiltration into the microstructures, then removal of excess wax, and (ii) heating at 100 °C for 3 h to redistribute the wax into a continuous low-surface-energy film. During melting, capillary forces draw the low-viscosity molten wax into the spaces between the pillars. Excess wax was removed after the first stage by manual agitation and wiping to avoid filling the spaces between the pillars and to preserve the microstructure. The samples were then air-cooled to room temperature at 25 °C, which solidified the wax into a hydrophobic coating over the microstructured surface. This carnauba wax coating process was repeated for the double wax coating samples.

Characterization

Surface morphology was examined by field-emission scanning electron microscopy (SEM; JEOL JSM-IT800) to evaluate microstructural fidelity and coating coverage. Three-dimensional surface topography was measured with a Keyence VHX-7000 digital microscope to obtain the areal height parameters and profile heights of the arrays. Arithmetical mean height (Sa) is the average absolute value of height deviations from the mean plane. Root mean square height (Sq) is the root mean square of the surface height deviations from the mean plane, representing the standard deviation of the surface heights. Measurements were acquired using a 50× objective lens over a 4000 µm × 4000 µm area, with five replicate measurements performed per sample. Surface chemistry was characterized by Fourier-transform infrared (FTIR) spectroscopy with an attenuated total reflectance (ATR) accessory (PerkinElmer Frontier).

Static water contact angles were measured at room temperature using a Theta Lite optical tensiometer, with data analysis performed via OneAttension software. A 5 µL droplet of distilled water was placed gently on the surface, and the angle was recorded 5 s after deposition, when the droplet had stabilized. Contact angles are reported as the mean ± standard deviation (SD); the minimum and maximum values were also examined to assess variability.

Wetting was related to the microstructure and the surface chemistry in order to establish structure–property relationships. Figure 3 shows the experimental workflow: fabrication of the flat reference and micropillar arrays by SLA, surface modification by alkali treatment and single or double carnauba wax coating, and followed by surface characterization.

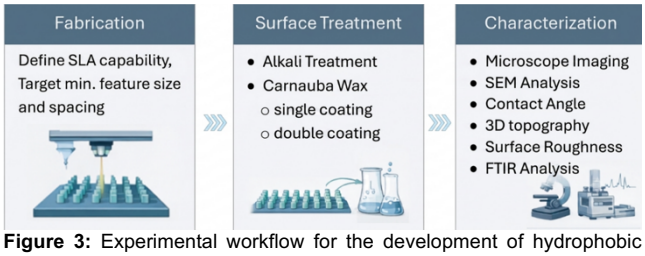


Figure 3: Experimental workflow for the development of hydrophobic micropillar arrays: sample fabrication, surface modification, and characterization.

RESULTS AND DISCUSSION

Micropillar Geometry

Fabricating the microstructured surfaces revealed several limitations of the Formlabs Form 2 SLA printer (Figure 4). Cylindrical and inverted conical pillars showed unintended curing of resin between the pillars, caused by light scattering, limited lateral resolution, and overcuring, which are inherent to photopolymerization. As a result, several designs could not be fabricated, particularly those with small spacings (100 µm). Pillars with 100 µm spacing showed significant resin bridging and fusion, while larger spacings (above 300 µm) were unsuitable because water could not be retained effectively within the array. Of the geometries evaluated, conical pillars had the highest print fidelity, with well-defined structures and minimal resin bridging.

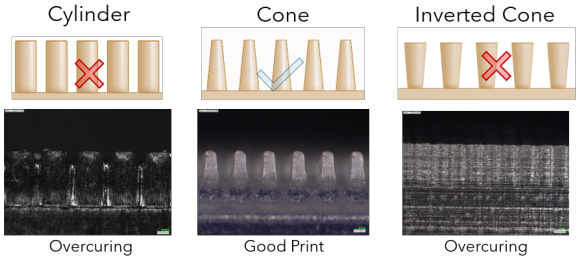


Figure 4: Print fidelity of conical pillars, which were more accurate than cylindrical and inverted conical pillars.

Print orientation strongly affected fabrication quality. Samples printed at 0° showed overcuring between adjacent pillars, whereas a 30° build orientation eliminated resin bridging and improved feature resolution. The improved fidelity is attributed to reduced light bleeding (Figure 5), in which scattered light propagates into the surrounding uncured resin and polymerizes it unintentionally. Tilting the structure by 30° reduces the cross-sectional area exposed in each layer, which limits lateral light propagation and preserves the designed geometry (Naik and Kiran, 2018).

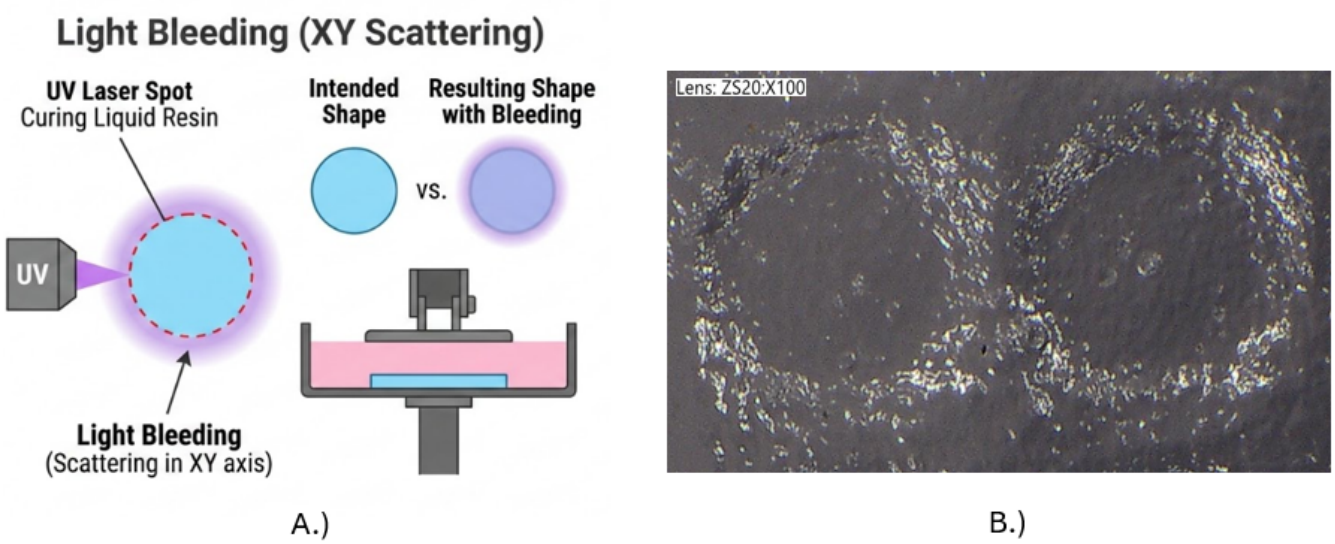


Figure 5: Light bleeding in stereolithography. (a) diagram of lateral (XY) laser scattering, in which the cured shape (outer halo) exceeds the intended shape. (b) Microscope image (100×) showing uncontrolled curing and coalescence of features caused by light bleeding.

Although the 30° orientation improved print quality, it caused a slight inclination of the pillars toward the tilt direction, owing to layer-by-layer fabrication and resin flow. To compensate, an additional 100 µm of spacing was added to the design at y-axis. The final pillar spacing was therefore set at 200 µm along the x-axis and 300 µm along the y-axis, which separated the pillars adequately and prevented them from merging during printing. The tilted orientation also produced microscale roughness through the staircase effect (Figure 6), giving a hierarchical surface texture that can enhance hydrophobicity (Bonilla-Cruz et al., 2021).

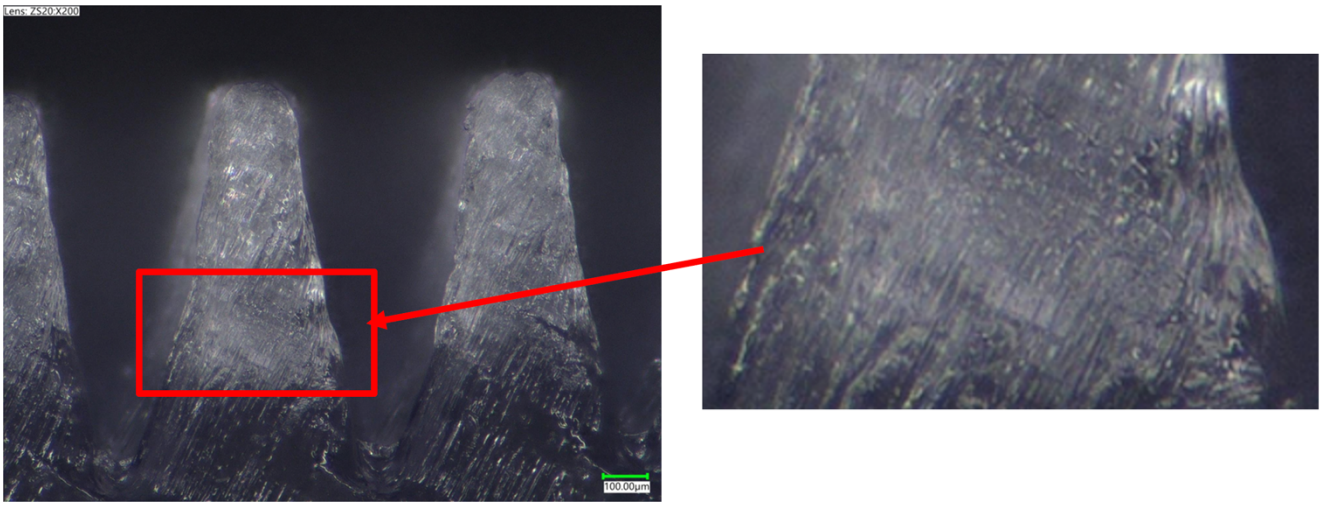


Figure 6: Changing the print angle produces different staircase patterns, which add micro-roughness (visible at 200× magnification).

Effects of Pillar Geometry and Chemical Modification

Figure 7 shows how pillar height and surface treatment affect the wetting of the SLA-printed microstructured surfaces. Overall, taller pillars generally gave more hydrophobic surfaces, but the effect depended strongly on the surface treatment.

Pillar Height	Untreated	Alkali	Single Coating Carnauba Wax	Double Coating Carnauba Wax
0 µm	CA = 67.17 ± 3.91	CA = 72.40 ± 0.97	CA = 85.80 ± 4.54	CA = 100.19 ± 3.88
200 µm	CA = 76.09 ± 4.06	CA = 83.30 ± 3.38	CA = 95.46 ± 3.00	CA = 100.46 ± 3.52
400 µm	CA = 93.48 ± 3.31	CA = 84.78 ± 2.39	CA = 107.97 ± 2.57	CA = 102.13 ± 4.16
600 µm	CA = 107.61 ± 3.33	CA = 84.10 ± 1.79	CA = 112.00 ± 6.34	CA = 108.83 ± 6.43
800 µm	CA = 103.01 ± 3.02	CA = 84.10 ± 1.88	CA = 136.98 ± 6.67	CA = 108.17 ± 3.39
1000 µm	CA = 97.13 ± 3.86	CA = 86.16 ± 1.37	CA = 140.72 ± 12.84	CA = 111.74 ± 1.16

Figure 7: Static water contact angle on the flat and micropillar surfaces as a function of pillar height and surface treatment (mean ± SD, n = 6)

On the untreated surfaces, increasing the pillar height first caused a pronounced increase in the contact angle. The flat SLA resin surface had a contact angle of 67.17° ± 3.91°, which rose to 107.61° ± 3.33° at a pillar height of 600 µm. This increase can be attributed to the micropillars and to the air pockets that form between adjacent pillars and reduce the solid–liquid contact area. The increase in hydrophobicity with pillar height therefore suggests that the microstructured geometry promoted air trapping (a partially non-wetted state). However, increasing the pillar height beyond 600 µm slightly decreased the contact angle to 103.01 ± 3.02 for 800 µm and 97.13 ± 3.86 for 1000 µm height. This may indicate that water penetrates the microstructure locally and that the contact line is pinned more strongly on taller pillars (Forsberg et al., 2010). At high aspect ratios, light bleeding, overcuring, and feature broadening in stereolithography may also make the pillars deviate from the intended geometry. Such deviations can change the effective spacing and aspect ratio of the microstructure and thereby reduce hydrophobicity.

In contrast to the untreated surfaces, alkali treatment gave substantially lower contact angles at all pillar heights, from approximately 72° to 86°. The reduction in hydrophobicity suggests that the chemical change outweighed the effect of the geometric roughness. Alkali treatment may hydrolyze the ester groups of the polymer network, forming or exposing polar hydroxyl and carboxyl groups at the surface. The geometric roughness of the micropillars was therefore insufficient to offset the greater intrinsic hydrophilicity caused by the alkali treatment.

Carnauba wax coating, on the other hand, produced a different response. Unlike the alkali treatment, which increased wetting, the wax coating greatly increased the hydrophobicity of the micropillar surfaces. Among the wax-coated specimens, the sample with 1000 µm pillars had a mean static water contact angle of 140.72° ± 12.84°, and the highest individual measurement was approximately 163°. The much higher contact angle than on the flat SLA surface and on the untreated microstructured surfaces indicates that the combination of low-surface-energy carnauba wax and micropillar geometry was particularly effective in reducing water-surface interaction. The double carnauba wax coating, however, exhibited a lower mean static contact angle of 111.74° ± 12.84° for the sample with 1000 µm pillars.

The increase in hydrophobicity after wax coating can be attributed to the intrinsically hydrophobic wax chemistry together with the surface features created by the microstructure and the wax deposit. The micropillars reduce the solid–liquid contact, while the wax coating lowers the affinity of the surface for water. This combination is a plausible explanation for the much higher contact angles of the wax-coated microstructured surfaces than of the untreated or alkali-treated ones.

Although individual contact angles exceeded 150°, a common criterion for superhydrophobicity, a static contact angle alone cannot establish superhydrophobic behavior or droplet mobility. The surfaces are therefore described as highly hydrophobic rather than superhydrophobic. The large difference between the mean and the maximum contact angle also indicates spatial variation in wetting across the surface. This variability may be associated with non-uniform wax deposition, local differences in surface roughness, and printing deviations in pillar dimensions, particularly for taller pillars.

Together, the results indicate that micropillar geometry and surface chemistry play complementary but distinct roles in controlling the wetting of SLA-printed surfaces. Geometry mainly determines the solid–liquid contact and the ability of the surface to retain air, whereas chemical modification determines its intrinsic affinity for water. The highest hydrophobicity was obtained when the micropillar array was combined with the low-surface-energy carnauba wax coating. Figure 8 summarizes the relationship among pillar height, surface treatment, and wetting.

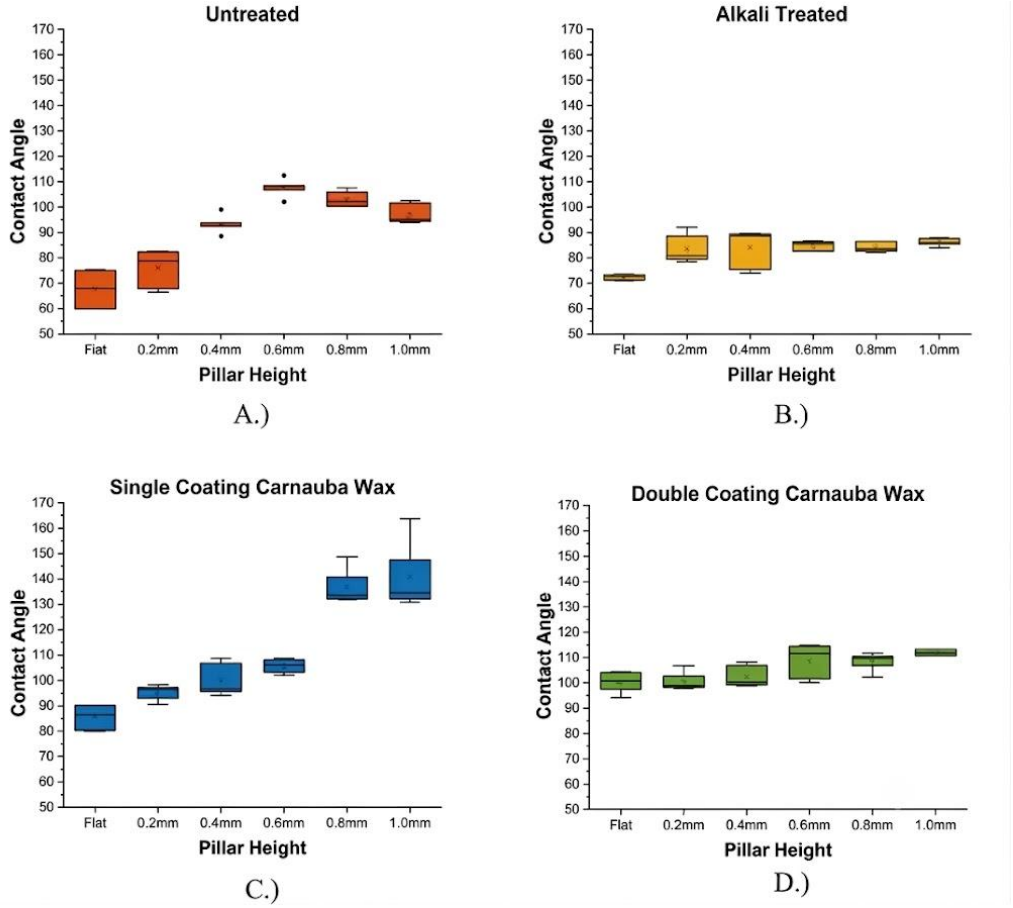


Figure 8: Distributions of the contact angle as a function of pillar height for SLA-printed surfaces with different treatments: (a) untreated, (b) alkali-treated, (c) single carnauba wax coating, and (d) double carnauba wax coating.

Surface Topography and Morphology

Three-dimensional surface topography was measured with a Keyence VHX-7000 digital microscope over a 4000 µm × 4000 µm field of view. The areal parameters Sa and Sq were calculated from the height maps. Because the measured area contained many micropillars, Sa and Sq describe the combined height variation of the printed microstructure and its surface texture, not nanoscale or sub-microscale roughness alone. The pillar geometry, particularly the pillar height, therefore contributes substantially to the measured

height distribution. No high-pass filter or plane correction was applied to the height maps.

To compare the surface treatments, the configuration with 1000 µm pillars was used throughout, because it gave the highest contact angle. Figure 9 shows the effect of surface treatment on the areal height parameters. The alkali treatment slightly increased the areal height, with Sa rising from 141.28 µm for the untreated surface to 149.79 µm. This increase may be due to the removal or modification of loosely bound surface material, which exposed or accentuated features of the printed surface. The largest values were obtained after a single carnauba wax coating, for which Sa and Sq rose to 173.03 µm and 210.29 µm, respectively.

In contrast, a second wax coating substantially reduced Sa and Sq, to 107.79 µm and 143.58 µm, lower than the single coating for about 37.7% and 31.7%, respectively. SEM and profilometry suggest that this reduction was caused by excess wax between the pillars, which partly filled the valleys and smoothed the geometric features. Rather than forming another conformal layer, the second coating therefore appears to have filled the valleys and planarized the surface. This interpretation is consistent with the blunted pillar profiles in the 3D topography and SEM images. In terms of wetting, the single wax coating therefore retained more of the hierarchical surface structure, whereas the double coating reduced the effective geometric roughness and thus changed the wetting mechanism.

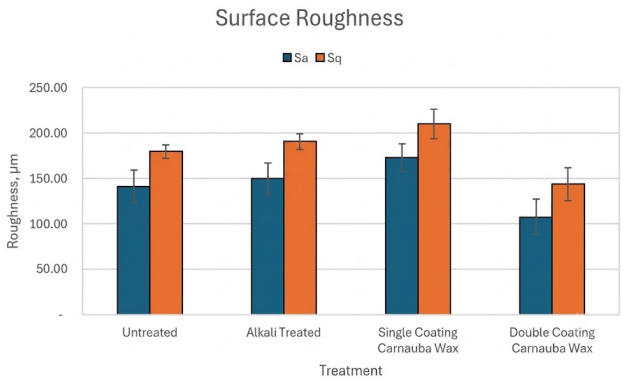


Figure 9: Arithmetic mean height (Sa) and root-mean-square height (Sq) for the untreated, alkali-treated, single carnauba wax-coated, and double carnauba wax-coated surfaces (1000 µm pillars, 4000 × 4000 µm field)

Figure 10 further illustrates the morphology of the surfaces under the four treatments. The 3D topography shows that the periodic arrangement of the printed micropillars remained generally intact after each treatment, with no sign of macroscopic pillar collapse or buckling. However, the overall peak-to-valley profile height changed measurably. After alkali treatment, the maximum profile height decreased by 5.72%, from 992.01 µm to 935.23 µm. After a single carnauba wax coating, the profile height partly recovered, to 973.65 µm, which suggests that the wax layer added to the measured height without substantially changing the pillar geometry. In contrast, the double-coated surface showed a pronounced 19.87% reduction in profile height, to 794.88 µm.

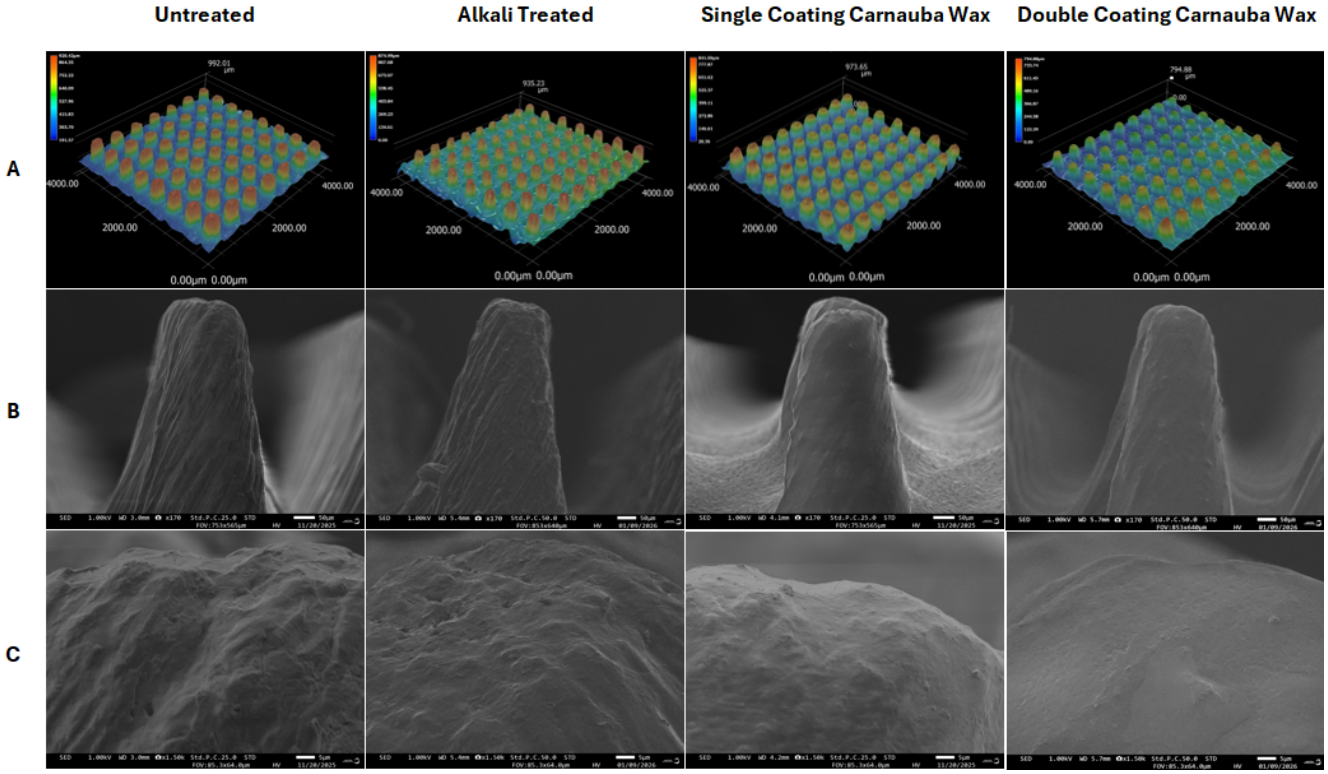


Figure 10: Fabricated microstructures under the four treatments: (a) 3D surface profile acquired with a Keyence VHX-7000 digital microscope over a 4000 × 4000 µm field of view; (b) SEM micrograph at 170× magnification; (c) SEM micrograph at 1500× magnification.

The large reduction in profile height after the second coating further supports a change from predominantly conformal coating to valley filling. The amount of deposited wax probably accumulated in the valleys between the pillars through wetting, capillary action, and gravity. Filling these regions raises the effective base plane and reduces the height difference between the pillar tips and the surrounding valleys. As a result, the effective macro-scale roughness and the aspect ratio of the array are reduced. This behavior provides morphological evidence for the valley-filling mechanism that was inferred from the reduced Sa and Sq and the blunted pillar profiles.

The SEM images support the 3D topography results, showing progressive changes in the pillar profiles and sidewall features. The

untreated and alkali-treated surfaces showed pronounced periodic staircase striations and micro-ridges, characteristic of layer-by-layer SLA printing. After a single carnauba wax coating, the sharp printing-related features became less pronounced as the wax wetted the polymer surface and filled the micro-grooves. This produced a more continuous surface while largely preserving the pillar geometry. With the second wax coating, however, the morphology changed more: the previously sharp truncated-cone pillar tips became rounded and blunted, and the sidewall textures were largely hidden by the thicker wax layer. These observations agree with the profilometry results and indicate that excess wax progressively masks the original SLA-generated microstructure.

Overall, the surface treatments produced two distinct morphological regimes. A single carnauba wax coating enhanced the microscale surface texture and kept the micropillar architecture, giving a greater measured roughness and preserving the hierarchical surface structure. In contrast, the double coating caused substantial wax accumulation between the pillars, leading to partial planarization, reduced effective roughness, and pronounced rounding of the pillar features. These morphological differences matter for the interpretation of wetting because wetting depends on both the surface chemistry and the presence of geometric features that can trap air beneath a water droplet.

Surface Chemistry

Figure 11 shows the FTIR spectra of the treated surfaces and of pure carnauba wax. The spectra show that the chemical structure of the methacrylate polymer is largely preserved after both alkali treatment and wax coating, and that additional bands of carnauba wax appear after coating, indicating that wax is present at the surface.

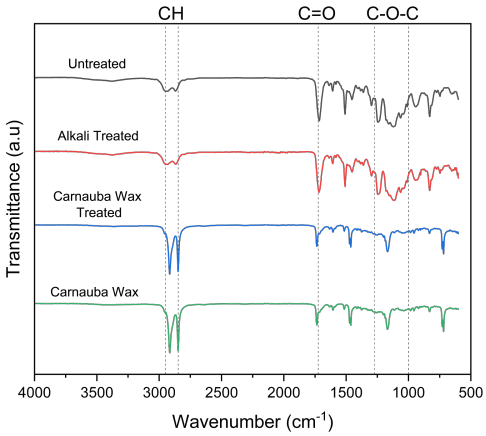


Figure 11: Normalized FTIR spectra of the untreated, alkali-treated, and carnauba wax-coated samples and of pure carnauba wax

The untreated polymer shows the characteristic bands of a methacrylate material. Weak bands at about 2950–2850 cm^{-1} correspond to the asymmetric and symmetric stretching vibrations of aliphatic C–H groups. The strong absorption at approximately 1730 cm^{-1} is assigned to the ester carbonyl (C=O) stretching vibration and is the most prominent band. The fingerprint region between 1260 and 1000 cm^{-1} is dominated by the C–O–C stretching vibrations of the ester linkage. These bands are consistent with the expected structure of methacrylate-based photopolymer resins.

After alkali treatment, the overall spectral profile is nearly identical to that of the untreated sample. This indicates that the treatment does not change the bulk chemical composition of the cured methacrylate network. Only slight changes in the intensity of the carbonyl band (~1730 cm^{-1}) and slight broadening of the ester band (~1260–1000 cm^{-1}) are evident.

The spectrum of pure carnauba wax shows strong absorptions at 2915 and 2848 cm^{-1}, corresponding to the asymmetric and symmetric stretching of long-chain aliphatic CH_2 groups and reflecting the high content of wax esters and long-chain fatty compounds. A carbonyl absorption appears near 1735 cm^{-1} from the ester groups naturally present in carnauba wax. Additional bands near 1460 cm^{-1} are attributed to CH_2 bending, and intense peaks between 1170 and 1040 cm^{-1} arise from ester C–O–C stretching. These bands are characteristic of natural waxes composed mainly of long-chain esters (Chaparro et al., 2023)

The wax-coated polymer shows spectral features from both the methacrylate substrate and the wax coating. Compared with the untreated surface, the coated sample shows a pronounced increase in the intensity of the C–H stretching bands at 2915 and 2848 cm^{-1}, matching those of pure carnauba wax. Likewise, the enhanced absorption at 1170–1040 cm^{-1} corresponds to the ester C–O–C stretching of the deposited wax. The carbonyl peak near 1730 cm^{-1} remains without appreciable shift, which suggests that the wax does not react chemically with the methacrylate polymer and forms a physically adhered layer. The similarity between the coated sample and pure carnauba wax confirms that the bio-based wax was deposited on the polymer surface

CONCLUSION

This study designed, fabricated, and surface-modified highly hydrophobic micropillar arrays by SLA 3D printing and carnauba wax coating. Of the pillar geometries evaluated, conical pillars had the highest print fidelity and structural integrity, with the least light bleeding, overcuring, and resin bridging. A 30° build orientation combined with extra spacing in the design minimized lateral resin fusion and kept the features separate. Combining micro-scale roughness with a low-surface-energy coating turned the hydrophilic baseline photopolymer (θ = 67.17°) into a highly hydrophobic surface (θ = 140.72°). For untreated surfaces, the contact angle peaked at a pillar height of 600 µm and then decreased slightly; for the wax-coated surfaces, the highest mean angle was at the tallest height tested, 1000 µm. The best-performing sample, single wax coating with 1000 µm pillars, reached a mean contact angle of 140.72° ± 12.84°. Combining SLA microstructuring with a natural carnauba wax coating is therefore a feasible way to make highly hydrophobic surfaces.

However, confirming a mobile Cassie–Baxter state requires measurement of the dynamic contact angles and droplet roll-off. Bio-based wax coatings are effective surface modifiers for enhancing hydrophobicity, but their mechanical durability was not evaluated and is expected to be limited.

Future work should evaluate their long-term durability under repeated wetting, running water, and abrasion, and should include dynamic contact-angle measurements.

ACKNOWLEDGMENTS

This work was supported by the Department of Science and Technology (DOST) – Philippine Council for Industry, Energy, and Emerging Technology Research and Development (PCIEERD) under the project “Materials for Application-Specific Technologies for 3D/4D Printing R&D (MAST3R)”. The author thanks the Advanced Device and Materials Testing Laboratory (ADMATEL) for the laboratory facilities and equipment used in this research. The author also thanks Dr. Marianito T. Margarito and Jenny Lyn Laga Alfeche for their guidance throughout this study.

CONFLICT OF INTEREST

The author declares no conflict of interest.

CONTRIBUTIONS OF INDIVIDUAL AUTHORS

M.P.R. conceived the study, performed the experiments and analysis, and wrote the manuscript.

REFERENCES

Bonilla-Cruz J, Sy JAC, Lara-Ceniceros TE, Gaxiola-López JC, García V, Basilia BA, and Advincula RC. Superhydrophobic μ-pillars via simple and scalable SLA 3D-printing: the stair-case effect and their wetting models. Soft Matter 2021; 17(32):7524–7531. https://doi.org/10.1039/D1SM00655J

Cassie ABD, and Baxter S. Wettability of porous surfaces. Transactions of the Faraday Society 1944; 40:546–551. https://doi.org/10.1039/tf9444000546

Chaparro LM, Neira LF, Molina D, Rivera-Barrera D, Castañeda M, López-Giraldo LJ, and Escobar P. Biowaxes from palm oil as promising candidates for cosmetic matrices and pharmaceuticals for human use. Materials 2023; 16(12):4402. https://doi.org/10.3390/ma16124402

Forsberg PSH, Priest C, Brinkmann M, Sedev R, and Ralston J. Contact line pinning on microstructured surfaces for liquids in the Wenzel state. Langmuir 2010; 26(2):860–865. https://doi.org/10.1021/la902296d

Gupta S, Ivvala J, and Grewal HS. Development of natural wax-based durable superhydrophobic coatings. Industrial Crops and Products 2021; 171:113871. https://doi.org/10.1016/j.indcrop.2021.113871

Huang J, Qin Q, and Wang J. A review of stereolithography: processes and systems. Processes 2020; 8(9):1138. https://doi.org/10.3390/pr8091138

Naik D, and Kiran R. On anisotropy, strain rate and size effects in vat photopolymerization based specimens. Additive Manufacturing 2018; 23:100807. https://doi.org/10.1016/j.addma.2018.08.021

Pagac M, Hajnys J, Ma QP, Jancar L, Jansa J, Stefek P, and Mesicek J. A review of vat photopolymerization technology: Materials, applications, challenges, and future trends of 3D printing. Polymers 2021; 13(4):598. https://doi.org/10.3390/polym13040598

Pathreeker S, Chando P, Chen FH, Biria S, Li H, Finkelstein EB, and Hosein ID. Superhydrophobic polymer composite surfaces developed via photopolymerization. ACS Applied Polymer Materials 2021; 3:4661–4672. https://doi.org/10.1021/acsapm.1c00744

Saji VS. Wax-based artificial superhydrophobic surfaces and coatings. Colloids and Surfaces A: Physicochemical and Engineering Aspects 2020; 602:125132. https://doi.org/10.1016/j.colsurfa.2020.125132

Sandner B, and Bischof C. Dependence of alkaline hydrolysis of poly(methyl methacrylate) on the reaction medium. Angewandte Makromolekulare Chemie 1983; 115:207–219. https://doi.org/10.1002/apmc.1983.051150117

Wang X, Fu C, Zhang C, Qiu Z, and Wang B. A comprehensive review of wetting transition mechanism on the surfaces of microstructures from theory and testing methods. Materials 2022; 15(14):4747. https://doi.org/10.3390/ma15144747

Wenzel RN. Resistance of solid surfaces to wetting by water. Industrial & Engineering Chemistry 1936; 28:988–994. https://doi.org/10.1021/ie50320a024

Wu C, Wei X, Chen Y, Liu J, Guo C, Wang Q, and Liang SY. Surface wettability analysis and preparation of hydrophobic microcylindrical arrays by μ-SLA 3D printing. Journal of Manufacturing Processes 2022; 83:14−26. https://doi.org/10.1016/j.jmapro.2022.08.041

Young T. An essay on the cohesion of fluids. Philosophical Transactions of the Royal Society of London 1805; 95:65–87. https://doi.org/10.1098/rstl.1805.0005